

Research Article

Structure-Based Virtual Screening of Phytochemicals from *Phyllanthus Amarus* as Potent Inhibitory Phytocompounds Against Marburg Virus Disease

Neeharika Singh,¹ Prem Pal Singh²¹Department of Biotechnology, University Institute of Engineering & Technology (UIET), Kurukshetra, India²Department of Electronics and Communication Engineering, Government College of Bharatpur, Bharatpur, India

Abstract

Marburg virus is a deadly and highly contagious pathogen, infects both human and non-human primates, and causes life-threatening Marburg virus disease. So far, there have been 14 MAVD outbreaks since August 1967. Influenza-like illness, manifestations related to abdomen, hemorrhagic, respiratory, and vascular system are among the signs and symptoms of MVD. The protein VP 35 is a multifunctional viral protein and binds to the double-strand RNA through its RBD and masks the dsRNA, which is a key sign of virus infection, recognized by host proteins including RIG-I and MDA-5. Here, we have performed molecular docking and MD simulation studies and shown that phytochemicals stigmasterol ($\Delta G = -8.62$ kcal/mol) and methyl ursolate ($\Delta G = -9.29$ kcal/mol) isolated from *Phyllanthus amarus* showed biologically significant poses to block the binding site of VP35 protein. The MD simulation result analysis confirmed that the complex structure of stigmasterol with RBD of protein VP35 show stable conformational dynamics during the MD simulation while methyl ursolate shows certain fluctuations in RMSD at certain time point but later attain stability. Hence, *Phyllanthus amarus*, which contains multiple antiviral and antimicrobial phytochemicals could be a conceivable candidate in the search for a drug for the MVD.

Keywords: MVD, MARV, VP35, RBD, Molecular Docking, MDS

Cite This Article: Singh N, Singh PP. Structure-Based Virtual Screening of Phytochemicals from *Phyllanthus Amarus* as Potent Inhibitory Phytocompounds Against Marburg Virus Disease. *EJMA* 2023;3(1):23–32.

The acute, severe, and life-threatening Marburg virus disease (MVD) caused by Marburg virus (MABV), has its origins in Africa and infects both human and non-human primates. Marburg virus belongs to Filoviridae family^[1,2] which further comprises the three recognized genera Ebolavirus (ebolavirus), Marburgvirus (Marburgvirus), and Cuevavirus.^[3] Influenza-like illness, manifestations related to abdomen, central nervous system, hemorrhagic, respiratory, and vascular system are among the signs and symptoms of MVD. Anorexia, diarrhea, myalgia, abdominal pain, fatigue, mal-

aise, nausea, sore throat, maculopapular rash and vomiting are its common clinical symptoms. The range for the MVD incubation time is 7 to 21 days.^[4,5] With outbreaks still happening in Central Africa, including two outbreaks in Uganda in 2012 and 2014, MVD is still a hazard to human health worldwide. The World Health Organization included MVD along with EVD in the 2018 Priority Diseases List (<https://www.who.int/blueprint/priority-diseases/en/>)6. Prevention of MVD is largely based on avoidance of direct contact with infected people or contaminated materials.^[1]

Address for correspondence: Prem Pal Singh, Assistant Professor. Department of Electronics and Communication Engineering, Government College of Bharatpur, Bharatpur, India. Pin Code: 321303

Phone: +91 8349572145 **E-mail:** singhhanuman599@gmail.com

Submitted Date: January 30, 2023 **Revision Date:** January 30, 2023 **Accepted Date:** March 05, 2023 **Available Online Date:** June 23, 2023

©Copyright 2023 by Eurasian Journal of Medical Advances - Available online at www.ejmad.org

OPEN ACCESS This work is licensed under a Creative Commons Attribution-NonCommercial 4.0 International License.



There have been 14 MAVD outbreaks overall since the Marburg virus (MARV) initially occurred in August 1967 (Supplementary Table 1).^[7] MARV is a highly contagious and a deadly pathogen. The genome of MARV contains single strand (-) sense RNA of 17kb-19kb in length and encode seven distinct types of genes, which code for Nucleoprotein (NP), Virion Protein (VP35), VP40, Glycoprotein (GP), VP30, VP24 and RNA dependent RNA Polymerase (L).^[4] The nucleoprotein collaborates with the virion protein to carry out the transcription and replication of the MARV. It also plays a crucial function in the growth and development of the virion protein. The outer layer of MARV consists of membrane anchored spike proteins made up of glycoproteins which give it a rough appearance and are crucially important in the entry thereby causing pathogenicity. There is another protein called virion protein 35 (VP35) which is a multifunctional viral protein and can act as an important factor in the synthesis of viral RNA, having an antagonistic effect on the type I Interferon formation pathway of the RIG-I (Retinoic acid-inducible gene-I) like receptor.^[8,9]

The protein VP35 comprises a flexible N-terminal region (1–90 amino acids), a central coiled-coil oligomerization domain (91–130), a flexible linker fragment (131–210) and a C-terminal dsRNA-binding domain (RBD) (211–340 amino acids) (Fig. 1). The protein VP35 binds to the double-strand RNA through its RBD and masks the dsRNA, which is a key sign of virus infection, recognized by host proteins including RIG-I and MDA-5. Protein VP35 interferes with the recognition of dsRNA by backbone-sensing host immune sentry molecules and provides an additional direction for antiviral development. However, it has been shown that there are no licensed antivirals, vaccines or particular pharmaceutical formulations that can cure a person infected with MARV.^[10]

Taking note of it, many researchers across the world have

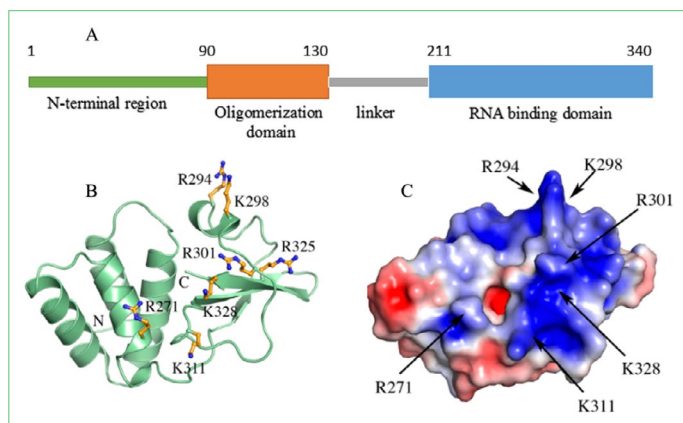


Figure 1. (a) Domain architecture of virion protein 35 (VP35) including N-terminal region, oligomerization domain (OD), linker and RNA binding domain (RBD) of protein VP35. (b) Cartoon representation of RBD and (c) Central basic patch residues of RBD of VP35..

shifted towards searching for answers in natural products. *Withania somnifera*, *Phyllanthus urinaria*^[11] *Azadirachta indica*,^[12] *Lycoris radiata*^[13] *Allium sativum*^[14] and many other species have been used for centuries for the treatment of cough, fever and cold and have also shown certain antiviral properties which opens door to explore their applications in drug design. *Phyllanthus amarus*, a small medicinal herb known as sleeping plant or Bhui korma in India, is an important plant in Indian traditional medicine belongs to the family Euphorbiaceae.^[15,16] It is used widely across the world for multiple diseases including treatment of jaundice, digestive disease and renal calculus.^[17,18] The phytochemicals isolated from *Phyllanthus amarus* have antibacterial, anticancer, antiviral, anti-inflammatory and antioxidant properties. Different parts of this plant are enriched in phytochemicals including flavonoids, alkaloids, tannins, lignans, tetraterpenes, sterols and many other compounds.^[14,18–24] It has been established that *Phyllanthus amarus* has promising antiviral activity against many viruses including Hepatitis B virus (HBV),^[25] Woodchuck Hepatitis Virus (WHV),^[26] R5 pseudotype HIV virus, Dengue Virus-2 and the Maloney-leukemia virus.^[27]

Hence, *Phyllanthus amarus*, which contains multiple antiviral and antimicrobial phytochemicals could be a conceivable candidate in the search for a drug for the MVD. Phytochemicals can be identified through structure-based virtual screening and further studying the molecular interactions, molecular dynamics simulation and ADME profiles of these extracts could shed light on whether compounds from *Phyllanthus amarus* could be used to target MVD.

Methods

Retrieval of Protein Structure

The crystal structure of RNA binding domain (RBD) of VP35 at 1.65 Å resolution with PDB ID: 4gh9 10 was downloaded from RCSB Protein Data Bank (PDB) (<https://www.rcsb.org/>) in the .pdb format.

Phytochemicals: Selection, Preparation and Pharmacokinetic Profiling

A thorough literature survey was done and a list of total 56 medicinal compounds extractable from *Phyllanthus amarus* was prepared (Table 1). The three dimensional (3D) chemical structures were taken from PubChem database (<https://pubchem.ncbi.nlm.nih.gov/>) and underwent geometry optimization using MMFF94 force field and steepest descent algorithm in 10000 steps, as implemented in Avogadro software.^[28] Physicochemical and pharmacokinetic properties of phytochemicals were obtained by SwissADME web-based server.^[29]

Table 1. List of phytochemicals and their docked energy score with RBD of VP35

Sr.No	PHYTOCHEMICALS	DOCKED SCORE (ΔG)	Sr.No	PHYTOCHEMICALS	DOCKED SCORE (ΔG)
1	Vanillic acid	-4.3	29	Quercetin	-6.2
2	P-coumaric acid	-4.5	30	Rhamnocitrin	-6.2
3	Methylgallate	-4.5	31	Tri-o-methylellagic acid	-6.3
4	Cinnamic acid	-4.7	32	Kaempferol-3-o-rutinoside	-6.4
5	Gallic acid	-4.8	33	Luteolin	-6.4
6	Phenazine	-5.3	34	Bursehernin	-6.5
7	Epibubbialine	-5.3	35	Prunin	-6.5
8	A-tocopherol	-5.4	36	Astragalin	-6.6
9	Securinol	-5.4	37	Rutin	-6.6
10	Phyltetralin	-5.4	38	Hinokinin	-6.7
11	Nor-securinine	-5.5	39	Myricetin 3-rhamnoside	-6.7
12	Niranthin	-5.5	40	Naringenin-7-O-glucoside	-6.7
13	Flavone, 4',5,7-triethoxy-3,3',6-trimethoxy	-5.5	41	Daucosterol	-6.8
14	Isobubbialine	-5.5	42	Kaempferol 3-glucuronide	-6.8
15	4-o-galloylquinic acid	-5.6	43	Quercetin 3-o-glucuronide isomer 2	-6.8
16	Phyllanthine	-5.6	44	Quercetin-3-o-glucoside	-6.8
17	Eriodictyol	-5.7	45	Quercitrin	-6.9
18	Naringenin	-5.7	46	Furosin	-7.0
19	Nirtetralin	-5.7	47	Quercetin 3-o-glucuronide isomer 1	-7.0
20	Gallocatechin	-5.7	48	Quercetin-3,4-di o-glucoside	-7.0
21	Securinine	-5.7	49	Lupeol	-7.2
22	Phyllanthin	-5.8	50	Furosin isomer	-7.3
23	Lintetralin	-6.0	51	Lupeol acetate	-7.3
24	Virgatusin	-5.8	52	Structure2D_Robinin	-7.4
25	Apigenin	-6.1	53	Corilagin	-7.5
26	Kaempferol	-6.1	54	Isocorilagin	-7.5
27	Phloridzin	-6.1	55	Stigmasterol	-8.62
28	Ellagic acid	-6.2	56	Methyl ursolate	-9.29

Molecular Docking

The preparation of both protein and ligand is a prerequisite for molecular docking. To do so, the "AutoDock Tool (ADT) 1.5.6" a molecular graphics laboratory user interface (MGL) was used.^[30] The RNA binding domain of protein VP35 was taken as an input file and water molecules, ions, and ligands were removed from the original structure file of the RBD. The polar hydrogen atoms and Kollman united atom charges were added to the RBD and the file was prepared in pdbqt format which is essential for the docking.^[31] Phytochemicals were prepared by adding the gasteiger charges and non-polar hydrogen atoms were merged.^[30] The pdbqt files were generated for all phytochemicals and further used for molecular docking. Based on the binding pocket,^[10] the grid box was defined for the ligand (phytochemical) docking on RBD of VP35 protein.

AutoDock Vina version 1.1.2 developed by Scripps Research Institute was utilized to perform molecular docking.^[32] The grid box parameters such as grid point (x, y, z: 70, 70, 70 Å,

respectively), grid center size (x, y, z: 14, 17, 4 Å, respectively) with a spacing of 0.375 Å, were defined in the binding pocket of the RBD of VP35 protein. The energy range, exhaustiveness, and the number of energy modes were taken as default values 4, 8, and 9, respectively. AutoDock Vina resulted in ligand conformations in the form of Gibbs free energy. The protein-ligand docked complexes and their interactions were visualized using PyMol and Biovia Discovery studio.^[33]

Molecular Dynamics Simulation

The molecular dynamics simulation (MDS) of best-docked complexes of protein from AutoDock Vina was performed using GROMACS v5.1.2.^[34] The SPC water model and GROMOS96 54a7 force field were used for the simulation of protein-ligand complexes. The ligand and protein topologies were generated by PRODRG web server^[35] and GROMACS, respectively. Further, ligand and protein topologies were combined to build the system topology. The cubic simulation box was created with a 10 Å buffer distance from the

centrally placed protein ligand complex. The system was solvated with SPC water molecules and neutralized by adding 0.15 M counter ions (Na⁺ and Cl⁻).^[36] During MD simulation the system energy was minimized with 50,000 steps for each steepest descent, followed by conjugate gradients. The MD simulation was performed at 300 K (physiological temperature). The SHAKE algorithm is used to satisfy bond geometry constraints such as maintaining constant bond angles or molecular rigidity, during molecular dynamics simulations. PME (Particle mesh Ewald) is a method for estimating electrostatic energies and forces of large periodic systems.^[37-39] The "SHAKE algorithm" was used to constrain all bonding which involves hydrogen and long-range electrostatic forces treated with PME. The system was equilibrated in NVT and NPT steps at 300 K for 500 picoseconds. Both temperature and pressure were maintained during the simulation using Berendsen thermostat^[40] and Parrinello-Rahman pressure.^[41,42] LJ potential with a cut-off of 0.10 nm was used for the van der Waals interactions. Following NPT ensemble, MD production runs were performed for the period of 50 nanoseconds. A 10 picoseconds time interval was set to update the energy, velocity, and trajectory. All MD production runs were done on DELL T7600 with a V100 GPU machine and Ubuntu Operating System. The GRO-MACS in-built utilities were utilized for the analysis of obtained molecular dynamics trajectories.

Results

Pharmacokinetics of Compounds

Potential drugs are those which satisfy the Pharmacokinetic and Pharmacodynamic properties with high safety margin. Thus, we determined which compounds from *Phyllanthus amarus* show an acceptable profile in terms of druggability and/or absorption/distribution/metabolism/excretion (ADME) properties. Violations from Lipinski's rule of five,^[43] predicted gastrointestinal absorption, and predicted drug-drug interactions were considered in picking the ligands for subsequent steps (Table 2).

Molecular Docking Analysis

The prepared ligands were docked to the protein's active site using AutoDock Vina software. The AutoDock Vina provides Gibbs free energy (ΔG) with various poses of ligands for each protein-ligand complex. The molar dissociation constant (Kd) was determined using the Gibbs free energy for the best-docked positions, which reflects the ligand's affinity for the receptor (i.e. RBD of VP35 protein). The Gibbs free energy values for all docked complexes are provided in Table 1. The best poses of ligands were found within the energy range of -7.0 to -9.29 Kcal/mol. On the basis of the Gibbs free energy (less than -7.5) and poses of

ligands, total four ligands including Corilagin, Isocorilagin, Stigmasterol and Methyl ursolate were considered for further structural analysis in PyMol, Chimera, and BIOVIA DS visualizer. Among these four compounds, corilagin ($\Delta G = -7.5$ kcal/mol) and isocorilagin ($\Delta G = -7.5$ kcal/mol) do not structurally fit into the binding pocket of RBD of VP35 while stigmasterol ($\Delta G = -8.62$ kcal/mol) and methyl ursolate ($\Delta G = -9.29$ kcal/mol) showed biologically significant poses to block the binding site of VP35 protein (Fig. 2). The stigmasterol interacts with the RBD with one hydrogen bond and nine hydrophobic interactions (Fig. 3a). Amino acid residue Threonine at 291 position of RBD of VP35 protein involved in the hydrogen bond formation with stigmasterol. The methyl ursolate interacts in the binding pocket with one hydrogen bond and nine hydrophobic interactions (Fig. 3b). The two dimensional structure of both stigmasterol and methyl ursolate are provided in Figure 4A & 4B.

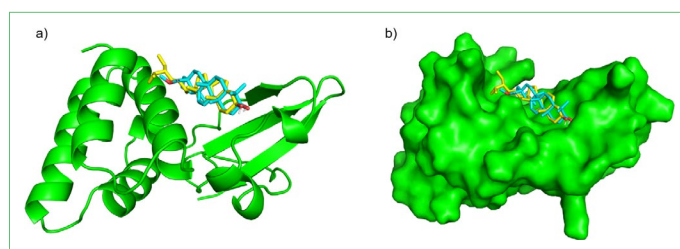


Figure 2. Protein-ligand interaction diagram (a) Cartoon view (b) Surface view. Both the phytochemicals nicely sit into the binding pocket of RBD of Protein VP35 (Stigmasterol; Cyan color, Methyl ursolate; Yellow color).

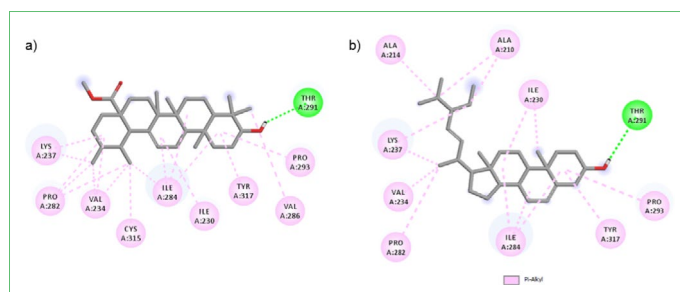


Figure 3. Two dimensional interaction diagram. (a) Stigmasterol (b) Methyl ursolate. Green and Magenta color represent hydrogen bond and Pi-Alkyl interaction.

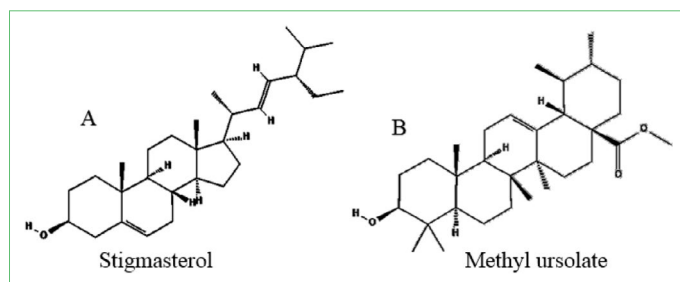


Figure 4. Two dimensional structure of Stigmasterol and methyl ursolate.

Table 2. ADME properties of phytochemicals used this study

Molecule Name	MW	Rotatable bonds	H-bond acceptors	H-bond donors	iLOGP	GI absorption	Lipinski violations
4-o-galloylquinic acid	344.27	4	10	7	-0.53	Low	1
Apigenin	270.24	1	5	3	1.89	High	0
Astragaln	448.38	4	11	7	1.29	Low	2
Bursehernin	370.4	6	6	0	2.96	High	0
Cinnamic acid	148.16	2	2	1	1.55	High	0
Corilagin	634.45	3	18	11	0.92	Low	3
Daucosterol	576.85	9	6	4	4.98	Low	1
Ellagic acid	302.19	0	8	4	0.79	High	0
Epibubbialine	221.25	0	4	1	1.87	High	0
Eriodictyol	288.25	1	6	4	1.62	High	0
Flavone, 4',5,7-triethoxy-3,3',6-trimethoxy Furosin isomer	444.47	10	8	0	4.62	High	0
Furosin	650.45	4	19	10	0.57	Low	3
Gallic acid	170.12	1	5	4	0.21	High	0
Gallocatechin	306.27	1	7	6	1.47	High	1
Hinokinin	354.35	4	6	0	3.08	High	0
Isobubbialine	221.25	0	4	1	1.86	High	0
Isocorilagin	634.45	3	18	11	1.51	Low	3
Kaempferol 3-glucuronide	462.36	4	12	7	1.23	Low	2
Kaempferol	286.24	1	6	4	1.7	High	0
Kaempferol-3-o-rutinoside	594.52	6	15	9	2.79	Low	3
Lintetralin	400.46	7	6	0	4.05	High	0
Lupeol acetate	468.75	3	2	0	4.89	Low	1
Lupeol	426.72	1	1	1	4.68	Low	1
Luteolin	286.24	1	6	4	1.86	High	0
Methyl ursolate	470.73	2	3	1	4.56	Low	1
Methylgallate	184.15	2	5	3	0.97	High	0
Myricetin 3-rhamnoside	464.38	3	12	8	1.61	Low	2
Naringenin	272.25	1	5	3	1.75	High	0
Naringenin-7-O-glucoside	434.39	4	10	6	2.35	Low	1
Niranthin	432.51	12	7	0	4.32	High	0
Nirtetralin	430.49	8	7	0	4.09	High	0
Nor-securinine	203.24	0	3	0	2.11	High	0
P-coumaric acid	164.16	2	3	2	0.95	High	0
Phenazine	180.21	0	2	0	2.19	High	0
Phloridzin	436.41	7	10	7	1.25	Low	1
Phyllanthin	418.52	13	6	0	4.26	High	0
Phyllanthine	247.29	1	4	0	2.41	High	0
Phytetralin	416.51	9	6	0	4.1	High	0
Prunin	434.39	4	10	6	2.35	Low	1
Quercetin 3-o-glucuronide isomer 1	478.36	4	13	8	1.37	Low	2
Quercetin 3-o-glucuronide isomer 2	478.36	4	13	8	1.13	Low	2
Quercetin	302.24	1	7	5	1.63	High	0
Quercetin-3,4-di o-glucoside	464.38	4	12	8	0.94	Low	2
Quercitrin	448.38	3	11	7	1.6	Low	2
Rhamnocitrin	300.26	2	6	3	2.31	High	0
Rutin	610.52	6	16	10	1.58	Low	3
Securinine	217.26	0	3	0	2.31	High	0
Securinol	235.28	0	4	1	2.19	High	0
Stigmasterol	412.69	5	1	1	5.01	Low	1
Robinin	740.66	8	19	11	2.99	Low	3
Tri-o-methylellagic acid	344.27	3	8	1	2.42	High	0
Vanillic acid	168.15	2	4	2	1.4	High	0
Virgatusin	416.46	8	7	0	4.02	High	0
A-tocopherol	430.71	12	2	1	5.92	Low	1

MD Simulation

Based on the molecular docking results obtained from AutoDock Vina, the stigmaterol and methyl ursolate compounds were taken for further molecular dynamic simulation. MD simulations of these two compounds were performed for the 50 nanoseconds at 300 K temperature. The Root Mean Square Deviation (RMSD) and Root Mean Square Fluctuations (RMSF) were analyzed to measure the deviation of alpha carbon atoms of the protein backbone and also the fluctuations associated with the amino acid residues of the protein during the simulation.^[44,45] The RMSD results of the RBD of VP35 protein complexed with stigmaterol, show quite stable conformational dynamics during the simulation of 50ns at 300 K temperature. The complex structure of stigmaterol with RBD of VP35 quickly attains equilibrium at RMSD ~ 0.18 nm during the initial 5–10 nanosecond, which is continued till 50 nanoseconds (Fig. 5a). The RMSF plot confirms that the average fluctuation of amino acid residues belonging to stable secondary conformations remains below 0.22 nm (Fig. 5b). The complex structure of methyl ursolate with RBD of VP35 quickly attains equilibrium at RMSD ~ 0.15 nm during the initial 0–2ns, which is continued till 20 ns. There is a slight displacement at 45ns but towards the end of simulation the

complexes become stable (Fig. 6a). The RMSF plot confirms that the average fluctuation of residues belonging to stable secondary conformations remains below 0.25 nm (Fig. 6b). The binding site residues for the RBD-phytochemical complexes from the RMSF plot show favorable molecular interactions and stable conformational dynamics of RBD-phytochemical complex interactions during simulation, which gives confidence to docking analyses.

Solvent-accessible surface area (SASA) of RBD-phytochemical complexes show the contribution of hydrophobic interactions of the nonpolar amino acids with the conformational stability of proteins in the solvent environment.^[45–47] The SASA results of the RBD of VP35 protein complex with stigmaterol and methyl ursolate for 50 ns simulation with an area of 65 nm² and 62 nm², respectively, show the stability of the RBD-phytochemicals conformation (Fig. 5e & 6e). The radius of gyration (Rg) of the RBD of VP35 protein complexed with stigmaterol and/or methyl ursolate complex indicates its conformational stability (Fig. 5d & 6d). Protein-phytochemical complexes are largely stabilized by the various inter and intra hydrogen bond interactions due to their role to accommodate the lead compound at the active site of a protein. Thus, we also calculated the evolution plot of H-bond interactions (Fig. 5c & 6c).

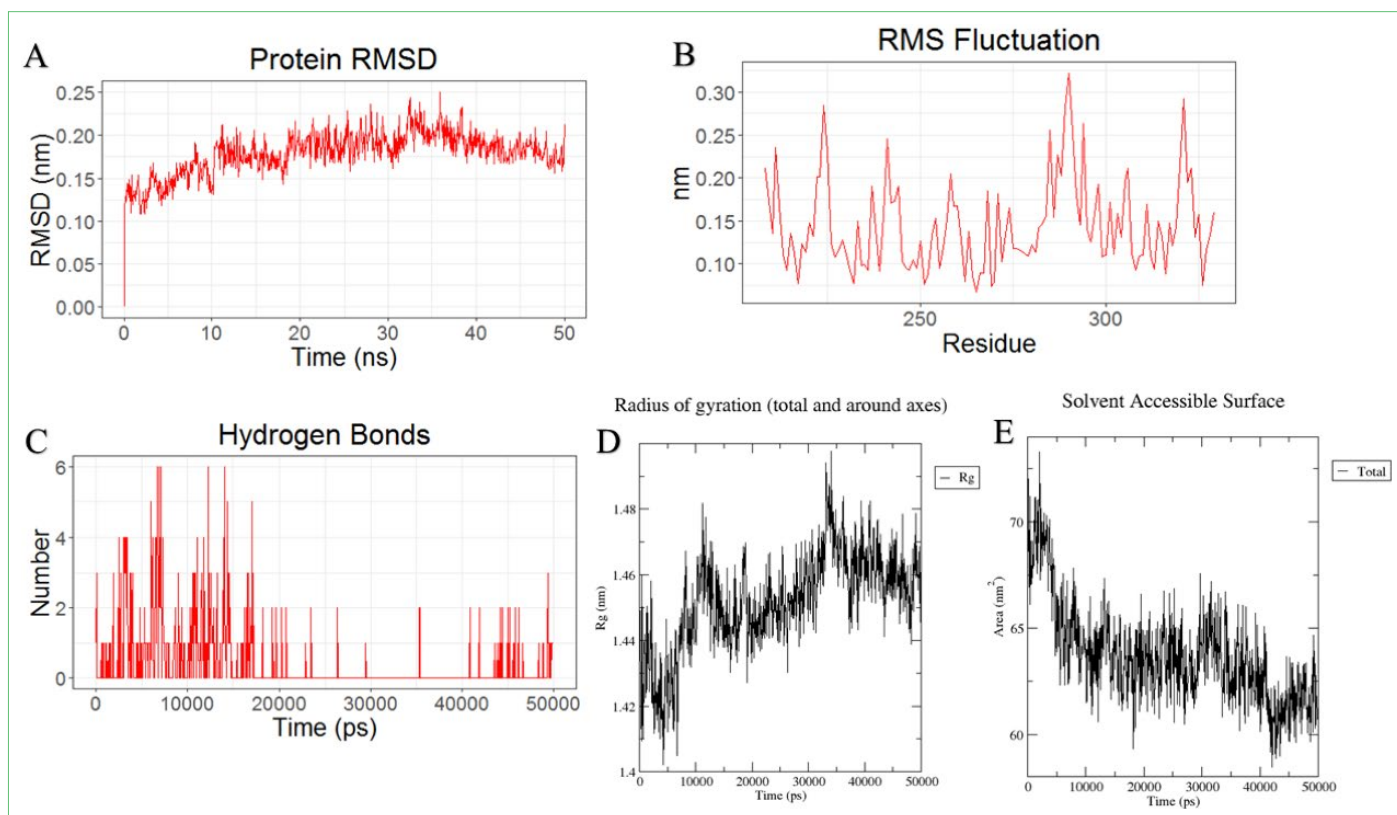


Figure 5. Molecular dynamics simulation diagram of Stigmaterol with protein VP35 RNA binding domain. The protein-ligand docked complex was simulated for 50 ns. (a) RMSD (b) RMSF (c) Hydrogen bonds (d) Radius of gyration (e) Solvent Accessible Surface Area.

Discussion

Many in-silico and experimental studies have been conducted in order to combat viral infections. In this study, we attempted to find potential inhibitors, and to do so, we selected the RBD of VP35 protein of MARV for the target. Marburg virus VP35 interferes with the recognition of dsRNA by backbone-sensing host immune sentry molecules. The protein VP35 binds to double strand (-) sense RNA through its RNA binding domain and masks the dsRNA, which is a key feature of virus infection that is identified by host proteins such as RIG-I and MDA-5. In this study, to predict potential inhibitors against VP35 protein we used in-silico approaches i.e. molecular docking followed by MD simulation. A total of 56 phytochemicals extractable from *Phyllanthus amarus* were taken from the PubChem database. For the preliminary screening of potential compounds, molecular docking was performed using AutoDock Vina. Based on molecular docking results, and structural analysis of docked compounds, we proceed with stigmasterol ($\Delta G = -8.62$ kcal/mol) and methyl ursolate ($\Delta G = -9.29$ kcal/mol) for further analysis. The binding interactions of these 2 compounds were investigated in PyMol and Biovia Discovery studio. The interactions of stigmasterol and methyl ursolate with VP35 protein are shown in figure 2 and 3. Other

compounds with high docking energy may also have the potential to block the RBD but to obtain the best potential candidate we proceed with only stigmasterol and methyl ursolate for molecular dynamics simulation. In comparison to methyl ursolate, stigmasterol has been investigated as a potential compound which fits well in the binding pocket and forms a more stable complex with RBD of protein VP35. The MD simulation result analysis which includes RMSD, RMSF, SASA, hydrogen bond analysis, and radius of gyration, confirmed that the complex structure of stigmasterol with RBD of protein VP35 show stable conformational dynamics during the MD simulation (Fig. 5) while methyl ursolate shows certain fluctuations in RMSD at certain time point but later attain stability which need to investigated for more time period (Fig. 6).

Targeting MARV via VP35 protein through phytochemical based drug can be a potential strategy against Marburg virus disease. Our computational work suggests that stigmasterol can be a potential lead compound against MVD. This study is based on computational methods and the conditions for the protein-phytochemical interaction in the computational study may differ from the physiological conditions, hence more detailed experimental work and clinical studies are required to establish the *Phyllanthus amarus* as a potential source to treat MVD.

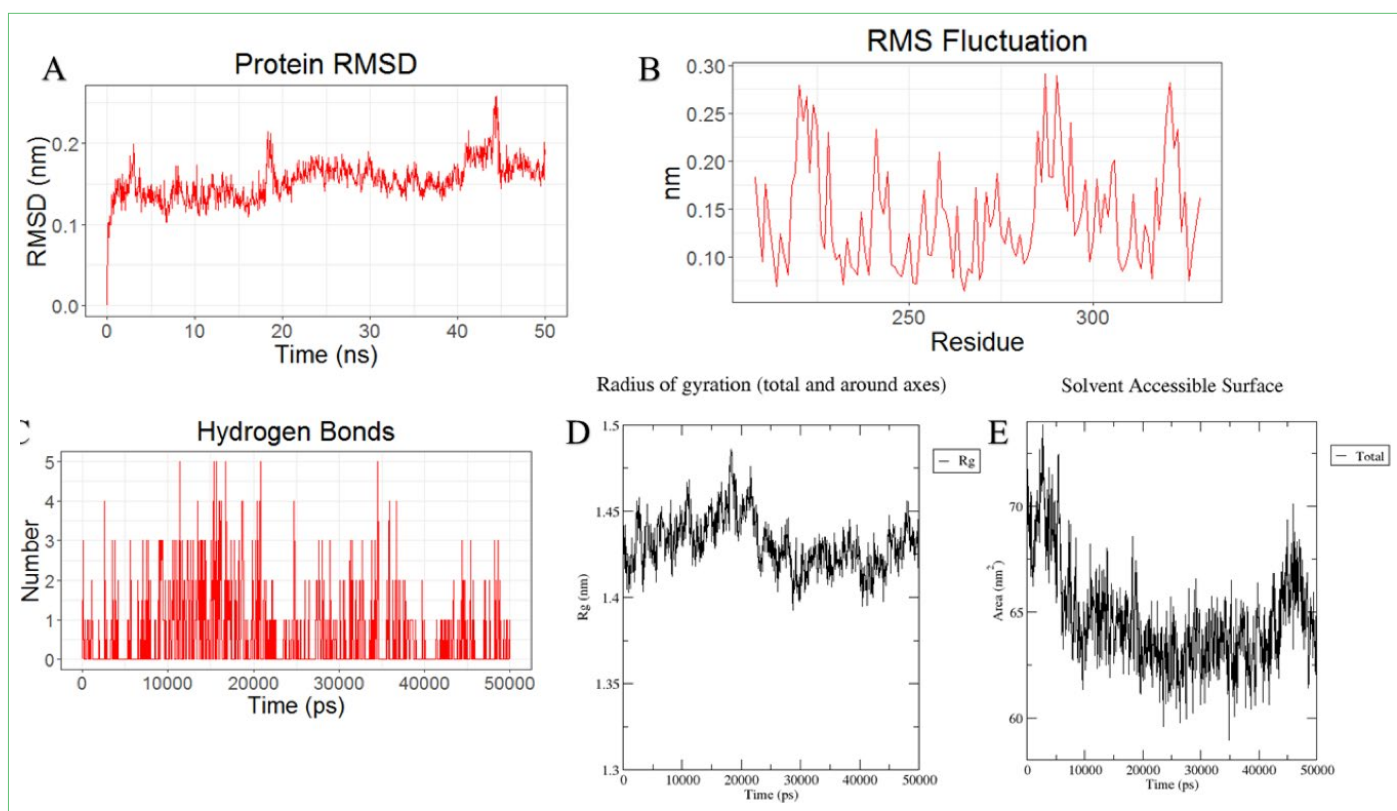


Figure 6. Molecular dynamics simulation diagram of Methyl ursolate with protein VP35 RNA binding domain. The protein-ligand docked complex was simulated for 50 ns. (a) RMSD (b) RMSF (c) Hydrogen bonds (d) Radius of gyration (e) Solvent Accessible Surface Area.

Conclusion

To find the potential compound against MARV, we used molecular docking and Molecular Dynamics Simulation. Out of 56 extractable phytochemicals from *Phyllanthus amarus*, stigmasterol and methyl ursolate showed the highest docking score with RNA binding domain of VP35 protein, and were considered for molecular dynamics simulation studies. In docking study, stigmasterol and methyl ursolate showed binding energy of -8.62 and -9.29 kcal/mol, respectively and MD simulation study showed RMSD value below 0.18 and 0.20 nm, respectively which indicates the very high stability of stigmasterol and methyl ursolate with RBD of VP35 protein. Our results suggest that *Phyllanthus amarus* can be a potent medicinal plant against MARV virus and stigmasterol can be taken as lead compound by pharma industry to design drug against MVD. However, in vitro and in vivo evaluation study is required to validate the efficacy and effectiveness of the compounds against MARV. The study may also lead to the synthesis of new derivatives stigmasterol and methyl ursolate which can be used effectively against RNA binding domain of VP35 protein of Marburg virus.

Disclosures

Peer-review: Externally peer-reviewed.

Conflict of Interest: None declared.

References

- Ristanović ES, Kokoškov NS, Crozier I, Kuhn JH, Gligić AS. A forgotten episode of marburg virus disease: Belgrade, Yugoslavia, 1967. *Microbiol Mol Biol Rev* 2020;84:e00095–19.
- Mavrakis M, Kolesnikova L, Schoehn G, Becker S, Ruigrok RW. Morphology of Marburg virus NP-RNA. *Virology* 2002;296:300–7.
- Nakayama E, Saijo M. Animal models for Ebola and Marburg virus infections. *Front Microbiol* 2013;4:267.
- Towner JS, Khristova ML, Sealy TK, Vincent MJ, Erickson BR, Bawiec DA, et al. Marburgvirus genomics and association with a large hemorrhagic fever outbreak in Angola. *J Virol* 2006;80:6497–516.
- Shifflett K, Marzi A. Marburg virus pathogenesis - Differences and similarities in humans and animal models. *Virol J* 2019;16:165.
- Olejnik J, Mühlberger E, Hume AJ. Recent advances in marburgvirus research. *F1000Res* 2019;8:F1000 Faculty Rev–704. .
- Brauburger K, Hume AJ, Mühlberger E, Olejnik J. Forty-five years of Marburg virus research. *Viruses* 2012;4:1878–927.
- Hariprasath R, Akashpriya C, Lakshmaiah VV, Praveen N. In silico studies of viral protein inhibitors of Marburg virus using phytochemicals from *Andrographis paniculata*. *J Appl Biol Biotechnol* 2022;11:222–31.
- Quazi S, Gavas S, Malik JA, Suman KS, Haider Z. In-silico pharmacophore and molecular docking based drug discovery against marburg virus's viral protein 35; A potent of MAVD. *bioRxiv*. 2021 Jul 3. Doi: 10.1101/2021.07.01.450693. [Epub ahead of print].
- Bale S. Marburg Virus VP35 Can Both Fully Coat the Backbone and Cap the Ends of dsRNA for Interferon Antagonism. *PLoS Pathog* 2012;8:e1002916.
- Yang CM, Cheng HY, Lin TC, Chiang LC, Lin CC. The in vitro activity of geraniin and 1,3,4,6-tetra-O-galloyl-beta-D-glucose isolated from *Phyllanthus urinaria* against herpes simplex virus type 1 and type 2 infection. *J Ethnopharmacol* 2007;110:555–8.
- Parida MM, Upadhyay C, Pandya G, Jana AM. Inhibitory potential of neem (*Azadirachta indica* Juss) leaves on dengue virus type-2 replication. *J Ethnopharmacol* 2002;79:273–8.
- Li SY, Chen C, Zhang HQ, Guo HY, Wang H, Wang L, et al. Identification of natural compounds with antiviral activities against SARS-associated coronavirus. *Antiviral Res* 2005;67:18–23.
- Mukhtar M, Arshad M, Ahmad M, Pomerantz RJ, Wigdahl B, Parveen Z. Antiviral potentials of medicinal plants. *Virus Res* 2008;131:111–20.
- Janghel V, Patel P, Chandel SS. Plants used for the treatment of icterus (jaundice) in Central India: A review. *Ann Hepatol* 2019;18:658–72.
- Patel JR, Tripathi P, Sharma V, Chauhan NS, Dixit VK. *Phyllanthus amarus*: ethnomedicinal uses, phytochemistry and pharmacology: a review. *J Ethnopharmacol* 2011;138:286–313.
- Ekor, M. Nephrotoxicity and nephroprotective potential of African medicinal plants. *Toxicological survey of African medicinal plants*. Elsevier; 2014. p. 357–93.
- Mao X, Wu LF, Guo HL, Chen WJ, Cui YP, Qi Q, et al. The genus *phyllanthus*: an ethnopharmacological, phytochemical, and pharmacological review. *Evid Based Complement Alternat Med* 2016;2016:7584952.
- Dhandapani R, Lakshmi D, Balakrishnan V, Jayakumar S, Kumar A. Preliminary phytochemical investigation and antibacterial activity of *Phyllanthus amarus* Schum & Thonn. *Anc Sci Life* 2007;27:1–5.
- Rajeshkumar NV, Joy KL, Kuttan G, Ramsewak RS, Nair MG, Kuttan R. Antitumour and anticarcinogenic activity of *Phyllanthus amarus* extract. *J Ethnopharmacol* 2002;81:17–22.
- Harikrishnan H, Jantan I, Haque MA, Kumolosasi E. Anti-inflammatory effects of *Phyllanthus amarus* Schum. & Thonn. through inhibition of NF- κ B, MAPK, and PI3K-Akt signaling pathways in LPS-induced human macrophages. *BMC Complement Altern Med* 2018;18:224
- Lim YY, Murtijaya J. Antioxidant properties of *Phyllanthus amarus* extracts as affected by different drying methods. *LWT - Food Science and Technology* 2007;40:1664–9.

23. Sarin B, Verma N, Martín JP, Mohanty A. An overview of important ethnomedicinal herbs of *Phyllanthus* species: present status and future prospects. *ScientificWorldJournal* 2014;2014:839172.
24. Zubair MF, Atolani O, Ibrahim SO, Adebisi OO, Hamid AA, Sowunmi RA. Chemical constituents and antimicrobial properties of *Phyllanthus amarus* (Schum & Thonn). *Bayero J Pure Appl Sci* 2017;10:238–46.
25. Lee CD, Ott M, Thyagarajan SP, Shafritz DA, Burk RD, Gupta S. *Phyllanthus amarus* down-regulates hepatitis B virus mRNA transcription and replication. *Eur J Clin Invest* 1996;26:1069–76.
26. Venkateswaran PS, Millman I, Blumberg BS. Effects of an extract from *Phyllanthus niruri* on hepatitis B and woodchuck hepatitis viruses: in vitro and in vivo studies. *Proc Natl Acad Sci U S A* 1987;84:274–8.
27. Sagar KS, Chang CC, Wang WK, Lin JY, Lee SS. Preparation and anti-HIV activities of retrojusticidin B analogs and azalignans. *Bioorg Med Chem* 2004;12:4045–54.
28. Hanwell M, Curtis DE, Lonie DC, Vandermeersch T, Zurek E, Hutchinson GR. Avogadro: an advanced semantic chemical editor, visualization, and analysis platform. *J Cheminform* 2012;4:17.
29. Daina A, Michielin O, Zoete V. SwissADME: a free web tool to evaluate pharmacokinetics, drug-likeness and medicinal chemistry friendliness of small molecules. *Sci Rep* 2017;7:42717.
30. Morris GM, Huey R, Lindstrom W, Sanner MF, Belew RK, Goodsell DS, et al. AutoDock4 and AutoDockTools4: Automated docking with selective receptor flexibility. *J Comput Chem* 2009;30:2785–91.
31. Vijesh AM, Isloor AM, Telkar S, Arulmoli T, Fun HK. Molecular docking studies of some new imidazole derivatives for antimicrobial properties. *Arab J Chem* 2013;6:197–204.
32. Trott O, Olson AJ. AutoDock Vina: improving the speed and accuracy of docking with a new scoring function, efficient optimization, and multithreading. *J Comput Chem* 2010;31:455–61.
33. DeLano WL. Pymol: An open-source molecular graphics tool. *{CCP4} Newsl. Protein Crystallogr* 2002;40:1–8.
34. Abraham MJ, Murtola T, Schulz R, Pall S, Smith JC, Hess B, et al. Gromacs: High performance molecular simulations through multi-level parallelism from laptops to supercomputers. *SoftwareX* 2015;1–2:19–25.
35. Schüttelkopf AW, van Aalten DM. PRODRG: a tool for high-throughput crystallography of protein-ligand complexes. *Acta Crystallogr D Biol Crystallogr* 2004;60:1355–63.
36. Joung IS, Cheatham TE 3rd. Determination of alkali and halide monovalent ion parameters for use in explicitly solvated biomolecular simulations. *J Phys Chem B* 2008;112:9020–41.
37. Ryckaert JP, Ciccotti G, Berendsen HJC. Numerical integration of the cartesian equations of motion of a system with constraints: molecular dynamics of n-alkanes. *J Comput Phys* 1977;23:327–41.
38. Durrant JD, McCammon JA. Molecular dynamics simulations and drug discovery. *BMC Biol* 2011;9:71.
39. Darden T, York D, Pedersen L. Particle mesh Ewald: An N-log(N) method for Ewald sums in large systems. *J Chem Phys* 1993;98:10089–92.
40. Berendsen HJC, Grigera JR, Straatsma TP. The missing term in effective pair potentials. *J Phys Chem* 1987;91:6269–71.
41. Parrinello M, Rahman A. Crystal structure and pair potentials: A molecular-dynamics study. *Phys Rev Lett* 1980;45:1196–9.
42. Hess B, Bekker H, Berendsen HJC, Fraaije JGEM. LINCS: A linear constraint solver for molecular simulations. *J Comput Chem* 1997;18:1463–72.
43. Lipinski CA. Lead- and drug-like compounds: the rule-of-five revolution. *Drug Discov Today Technol* 2004;1:337–41.
44. Kufareva I, Abagyan R. Methods of protein structure comparison. *Methods Mol Biol.* 2012;857:231–57
45. Mishra CB, Kumari S, Prakash A, Yadav R, Tiwari AK, Pandey P, et al. Discovery of novel Methylsulfonyl phenyl derivatives as potent human Cyclooxygenase-2 inhibitors with effective anticonvulsant action: Design, synthesis, in-silico, in-vitro and in-vivo evaluation. *Eur J Med Chem* 2018;151:520–32.
46. Bhowmik D, Jagadeesan R, Rai P, Nandi R, Guban K, Kumar D. Evaluation of potential drugs against leishmaniasis targeting catalytic subunit of *Leishmania donovani* nuclear DNA primase using ligand based virtual screening, docking and molecular dynamics approaches. *J Biomol Struct Dyn* 2021;39:1838–52.
47. Zhang X, Yan J, Wang H, Wang Y, Wang J, Zhao D. Molecular docking, 3D-QSAR, and molecular dynamics simulations of thieno[3,2-b]pyrrole derivatives against anticancer targets of KDM1A/LSD1. *J Biomol Struct Dyn* 2021;39:1189–202.

Supplementary Table 1. Number of cases and deaths reported across the world due to MAV from 1967 to 2021

Year(s)	Country	Origin	Cases	Number (%) of deaths	References
1967	Germany & Yugoslavia	Uganda	31	7 (23)	1, 2
1975	Johannesburg, South Africa	Zimbabwe	3	1 (33)	3
1980	Kenya	Kitum cave	2	1 (50)	4
1987	Kenya	Kitum cave	1	1 (100)	5
1990	Russia	Russia	1	1 (100)	6
1998-2000	Democratic Republic of Congo	Durba, DRC	154	128 (83)	7
2004-2005	Angola	Uige Province, Angola	252	227 (90)	8
2007	Uganda	Lead and gold mine in Kamwenge District, Uganda	4	2 (50)	9
2008	USA	Python cave (Uganda)	1	0	10
2008	Netherlands	Python cave (Uganda)	1	1 (100)	11, 12
2012	Uganda	Kabale	15	4 (27)	13
2014	Uganda	Kampala	1	1 (100)	14
2017	Uganda	Kween district	3	3 (100)	15
2021	Guinea	Guéckédou, Nzerekore Region	1	1 (100)	16